ORGANIC PROCESS RESEARCH & DEVELOPMENT
OPR&D
Article
Cite This: Org. Process Res. Dev. 2019, 23, 1948−1959
pubs.acs.org/OPRD

Isothermal by Design: An Accelerated Approach to the Prediction of the Crystallizability of Slowly Nucleating Systems

Peter L. Kaskiewicz,[†] Guangyi Xu,[†] Xiaojun Lai,[†] Nicholas J. Warren,[†] Kevin J. Roberts,*[,†] Colin Morton,[‡] Peter Dowding,[‡] and Neil George[§]

[†]School of Chemical and Process Engineering, University of Leeds, Leeds LS2 9JT, U.K.
[‡]Infineum UK Ltd, Milton Hill Business and Technology Centre, Abingdon OX13 6BB, U.K.
[§]Syngenta UK Ltd, Jealott's Hill International Research Centre, Berkshire RG42 6EY, U.K.

Supporting Information

ABSTRACT: A route to the accelerated nucleation of *α-para*-aminobenzoic acid in ethanol/water (EtOH/H_2O) mixed solvent solutions, using antisolvent crystallization, is presented. An *isothermal by design* approach is adopted, whereby the exothermic enthalpy of mixing associated with antisolvent addition is offset by the control of the temperature of the antisolvent added. Induction times (τ) are found to be reduced by 4 orders of magnitude using this methodology, consistent with the use of this approach as a nucleation acceleration technique. Calculation of the nucleation kinetic parameters for a range of solution concentrations, compositions, and supersaturations (S) reveal that effective interfacial tensions (γ_{eff}) vary from 8.4 to 2.3 mJ m^{-2} from solutions in H_2O solvent and EtOH solvent, respectively, in line with the trend in solubility. The critical nucleus radius (r^*) decreases from 1.98 to 0.40 nm associated with a decrease in the number of molecules in the critical nucleus (i^*) from 196 to 2 molecules. A change in nucleation mechanism from heterogeneous nucleation to homogeneous nucleation is observed to take place at $S \approx 1.5$. Limitations, particularly with focus toward larger-scale operation, are highlighted together with potential solutions to overcome such aspects.

KEYWORDS: *crystallization, nucleation, induction time, antisolvent, drown out, stability, kinetics, para-aminobenzoic acid*

1. INTRODUCTION

Crystallization is a highly energy-efficient key unit operation for isolation and purification in the manufacture of drugs, pigments, agrochemicals, confectionary, and other fine chemicals.[1] Nevertheless, crystallization can also be an unwanted phenomenon, for example, in cases such as fuels operating in cold weather or drugs stabilized in highly concentrated liquid formulations.[2]

The driving force for crystallization is supersaturation, and this process encompasses two distinct transformational stages—nucleation and growth.[3] In solution crystallization, nucleation signifies the structural pathway by which solute molecules cluster together to form 3-D nuclei; when these nuclei achieve a critical cluster size, termed the critical nucleus radius (r^*), with a defined number of molecules in the critical nucleus (i^*), growth is favored.

Nucleation can be divided into two categories: heterogeneous nucleation (HEN) and homogeneous nucleation (HON). HEN is caused when sites, usually suspended particles or impurities in the solution, provide a surface for nucleation, whereas HON describes spontaneous nucleation within the bulk solution.[4] Nucleation behavior can be modeled by classical nucleation theory (CNT), enabling the expression of the rate at which nucleation occurs (J) through an Arrhenius reaction rate equation[3]

$$J = A \exp\left[-\frac{16\pi\gamma^3 v_0^2}{3k^3T^3(\ln S)^2}\right] \quad (1)$$

which indicates that there are three main contributors to the rate of nucleation: temperature (T), degree of molar supersaturation (S), and interfacial tension (γ).[3] Further parameters in the equation include the pre-exponential factor, A, the volume occupied by a solute molecule in a crystal, v_0, and the Boltzmann constant, k.

Nucleation can occur in an infinitesimally short time frame or it can take a period of years. This uncertainty means that tests are currently performed to screen crystalline products, which might undergo nucleation events with significant impact upon product performance, such as polymorphic screening,[5] which includes solution crystallization using an array of solvents as well as relatively high supersaturation conditions. However, these tests cannot, as yet, predict if/when a nucleation event may take place over an extended period of time, which would constitute a "slowly nucleating system", because of the timescale of a nucleation event being longer than could be routinely tested under current realistic experimental time frames in both academic and industrial settings. There are a number of examples of slowly nucleating systems, including citric acid in water,[6] fats,[7] conversion of diamond to graphite, drug products,[8] etc. If tests could be implemented to predict this, then perhaps steps might be taken to mitigate an unforeseen nucleation event either through nucleation inhibition[9] or by formulating a different solid form.[10]

Received: May 23, 2019
Published: August 9, 2019

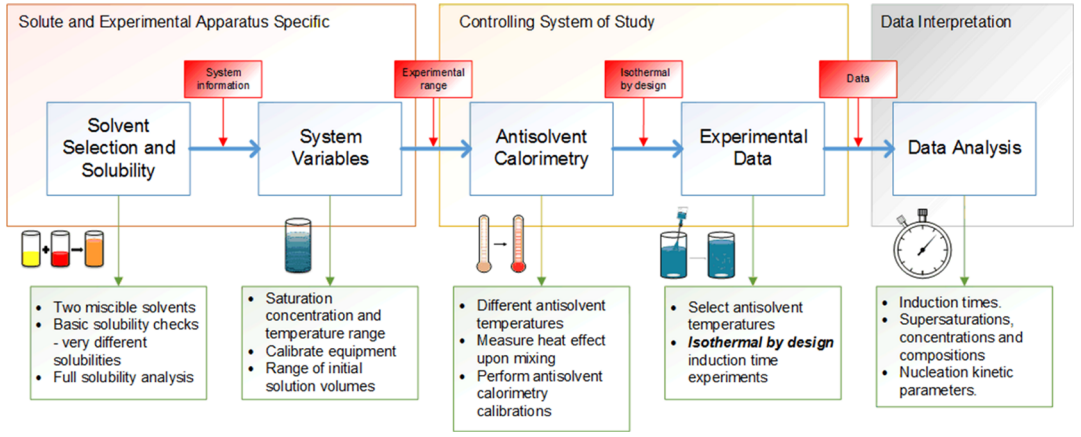

Figure 1. Workflow detailing the consistent steps required in order to perform the IbD approach for any system of study.

In chemical stability studies, accelerated approaches have been used in order to understand and hence predict properties, such as stability or reactivity, through the application of elevated thermodynamic conditions. In this, products are held at relatively high temperatures for a short period to emulate the effect of storage at room temperature for an extended period.[11] In a similar manner, an accelerated methodology could be employed to predict nucleation events of slowly nucleating systems, involving the process of increasing the rate of nucleation through solution crystallization at high supersaturations. Numerous avenues exist to try and achieve this, such as antisolvent crystallization (also known as drown-out crystallization),[12−14] crash cooling crystallization,[15] sono[16−18] and/or gassing[19,20] crystallization, or templated crystallization.[21−23] Each of these techniques produces a higher nucleation rate than could perhaps be achieved through standard crystallization processes, such as cooling, isothermal, or evaporative crystallization processes. Although each technique has different intricacies related to various methodological aspects, antisolvent crystallization has been shown to yield effective high supersaturation results with relative ease,[5,12] and therefore was used during this study.

In antisolvent crystallization, two completely miscible solvents, each with substantial difference in the solubility for the solute, are used. The solute is crystallized by isothermally adding the low solubility solvent (antisolvent) to a concentrated solution of the other, with the difference in solubility increasing the solution supersaturation and, as such, driving the crystallization process. Antisolvent crystallization has been studied extensively with a different focus on the effect it has upon certain crystallization systems, such as different addition flow rates,[24] solvent composition,[25] polymorphism,[26] crystal size distribution,[27] antisolvent control,[28] combined cooling and antisolvent crystallization (CCAC),[29] and antisolvent in continuous crystallizers.[30] Although this process has been well studied, a simple methodology to apply this approach to screen potential crystallizing systems and measure their kinetics has not, as of yet, been proposed.

A significant problem with performing antisolvent crystallizations for isothermal nucleation kinetic analysis, however, is that when a second solvent is added to a solution, there is usually an exothermic enthalpy of mixing, which can cause considerable increases in the overall solution temperature. Such variations in solution temperature can make it quite challenging to derive meaningful nucleation kinetics from the analysis of such data. This is particularly problematic for the case of crystallization at relatively high solution supersaturations, where crystallization occurs quite rapidly, and also where the enthalpy of mixing is much higher because of the greater amount of added antisolvent.

Because of the dynamics of heat transfer, regulation of reactor temperature is not really a feasible option for process-scale reactions given the difficulties associated with the homogeneity of solution temperatures in large-scale vessels, especially with fast changes in solution temperature, given the conductive heating control of reactor jackets.[2,31−34] An alternative approach is to offset the temperature of the antisolvent that is added to the solution in a manner so as to affect a heat balance associated with the enthalpy of mixing, hence ensuring both isothermal conditions and high supersaturations. This approach is described through the nomenclature—"isothermal by design" (IbD). The IbD concept is demonstrated in this paper through a study of the accelerated nucleation of α-*p*-aminobenzoic acid (pABA) from aqueous ethanol solution through an aqueous antisolvent addition. In such an experiment, the time to crystallize after antisolvent addition, the induction time (τ), can be measured to determine how quickly nucleation occurred. pABA in aqueous ethanol solution with an aqueous antisolvent was chosen for this study because of the large amount of work carried out on pABA in this research group providing data on key nucleation parameters and solubility effects to compare the current;[35−37] previous studies have determined that the metastable zone width of pABA was relatively large in the EtOH solvent, and as such, it could be used as a model system for the determination of a possible nucleation acceleration methodology and also as it represents a model pharmaceutical compound and solvent system. A good review of the crystallization science of pABA is described in a previous study.[35]

The structure of the paper is as follows:

After this introduction, the methodology workflow is presented, followed by results, discussion and conclusions.

2. MATERIALS AND METHODS

A workflow detailing the steps required for the IbD approach for any system of study is given in Figure 1.

2.1. Materials. pABA (99% pure) was supplied by Alfa Aesar, ethanol absolute (≥99.8% pure) was supplied by VWR, and deionized water was sourced on site at the University of Leeds.

DOI: 10.1021/acs.oprd.9b00242
Org. Process Res. Dev. 2019, 23, 1948−1959

2.2. Experimental Procedure. All the crystallization and dissolution experiments were carried out using the Technobis Crystal 16 system,[38] which records transmission data as a function of the temperature and time. A temperature calibration of the system was performed to ensure that correct temperature measurements were both taken and set under the experimental procedures undertaken.

Solubility of pABA in EtOH/H_2O mixed solutions was determined prior to antisolvent addition experiments. Solutions were prepared at a minimum of four solution concentrations, with the concentrations used dependent upon the solvent composition. Eleven solvent compositions ranging in 10 wt % increments of EtOH from pure EtOH to pure H_2O were used. Solutions were weighed on a balance with ±0.1 mg accuracy and heated to 333 K at 300 rpm for 1 h to ensure total homogenization of the solution. The solution (1 mL) was then transferred to 1.5 mL disposable glass vials for use in the experimental apparatus, which contained 7 mm × 2 mm magnetic stirrers, using a Fisherbrand 100−1000 μL micropipette with preheated pipette tips (303 K) to prevent unwanted crystallization.

The 1 mL solutions were subject to different cooling and heating cycles between 333 and 278 K at set rates (q, where q = 0.3, 0.5, 0.7, and 1 K min^{-1}), while stirring at 600 rpm. Crystallization (T_c) and dissolution (T_{diss}) temperatures as well as crystallization temperatures at the kinetic limit ($T_{c,l}$) and equilibrium saturation temperatures (T_e) were determined from transmission data, with the methodology undertaken to determine each of these parameters described in the previous literature.[39]

A van't Hoff analysis was performed from the obtained solubility data to determine how the system of study deviated from ideality, with the ideal solubility of pABA obtained from the previous literature,[36] based upon the Hildebrand equation (eq 2). Activity coefficients (Y) and enthalpy (ΔH_{diss}) and entropy (ΔS_{diss}) of dissolution were calculated based on the following equations, which have been derived in the previous literature[39]

$$\ln(x_{ideal}) = \frac{\Delta H_{fus}}{R}\left[\frac{1}{T} - \frac{1}{T_m}\right] \quad (2)$$

$$Y = \frac{x_{ideal}}{x} \quad (3)$$

$$\ln(x) = -\frac{\Delta H_{diss}}{RT} + \frac{\Delta S_{diss}}{R} \quad (4)$$

where x_{ideal} is the solution concentration, x is the experimentally measured molar solubility, ΔH_{fus} is the enthalpy of fusion, R is the ideal gas constant, T is the temperature, and T_m is the melting temperature.

For antisolvent calorimetry experiments, all solutions were prepared to ensure a saturation temperature of 293 K for a mixed solvent solution of 70 wt % EtOH:30 wt % H_2O EtOH/H_2O and pABA. This temperature was chosen at it was low enough to ensure minimal solvent evaporation during the experiments. The solvent composition was selected because of solubility studies highlighting that small additions of H_2O to pABA in EtOH solution increased the solubility, whereas over the temperature range used, any addition of H_2O to a 70 wt % EtOH:30 wt % H_2O composition only decreased the solubility, while providing a large range of solvent compositions to be examined in the performed experiments. Solution volumes used ranged from 0.80 to 0.20 mL in 0.05 mL increments, with all solution volumes made up to 1 mL after antisolvent addition.

Calibrations based upon solution calorimetry were performed to ensure an IbD approach, with 5 initial volumes selected for the calibration at a selected temperature (ranging from 293 to 301 K in 2 K increments), with four different antisolvent temperatures selected. Solutions were held at constant temperature, stirring at 900 rpm, with the antisolvent held at constant temperature, stirring at 700 rpm. The calibrations were performed by placing a digital thermometer into the solution vials and then withdrawing the full antisolvent volume with a 1 mL syringe with an attached needle and transferring the contents into the solution vial rapidly, inducing high mixing. The speed of addition meant that the antisolvent was added almost instantaneously, leading to this procedure being described as "instant addition". The temperature of the solution was recorded after each addition by taking the value of the highest recorded temperature on the digital thermometer within 1 s after antisolvent addition. Each calibration was repeated four times. Plots of selected antisolvent temperatures against the temperature of solutions after antisolvent addition were made and linear regressions were plotted with extrapolations to the desired solution temperature, indicating the required antisolvent temperature to maintain the solution temperature upon addition. This was then used to determine which antisolvent temperature should be used for each induction time experiment at that temperature. This was subsequently tested to ensure that the calibrations were accurate and that the solution temperatures were maintained upon addition of the antisolvent at the determined calibration temperatures. It was observed that deviations in solution temperature upon addition of H_2O, over a range of four repeats, were at most ±0.2 K, with solutions quickly returning to set temperatures in a manner of a few seconds. Therefore, this effect was deemed to be negligible.

After the calorimetry calibrations were completed, the induction time experiments were performed. The same procedure was undertaken as described for the calibrations, leading to an "instant addition" methodology; however, all selected solution volumes were used, antisolvent temperatures were selected based upon the calibrations, and no digital thermometer was placed in the vials, ensuring no effect on nucleation by introducing another surface on which to crystallize upon. Sixteen repeats were performed for each initial solution volume used at each selected temperature. The induction time to nucleation was determined from the collected transmission data.

The isothermal transmittance data were used to calculate the time between when the antisolvent was added to the vials and when nucleation had occurred, giving the induction time. The point at which the antisolvent was added was also determined by the transmission data. This process is described in Supporting Information S3, along with a more detailed description of the experimental procedures undertaken.

2.3. Analysis of Nucleation Kinetics and Mechanism. Molar supersaturations for each solution were calculated according to

$$S = \frac{c}{c^*} \quad (5)$$

where c is the absolute solute concentration and c^* is the saturation concentration.

DOI: 10.1021/acs.oprd.9b00242
Org. Process Res. Dev. 2019, 23, 1948−1959

The rate of nucleation was taken to be related to the induction time obtained from the experiments under the relationship described through the equation[3]

$$\tau \propto J^{-1} \tag{6}$$

The induction time data (τ as a function of S) were analyzed using CNT[4,40] according to

$$\ln\{\tau[S(S-1)^{md}]^{1/1+md}\} = \ln k_{md} + \frac{B}{[(1+md)(kT\ln S)^2]} \tag{7}$$

$$k_{md} = \left[\frac{(1+md)\alpha_{det}}{k_v z f_e^* c_s d_0^{\,d} f_{e,s}^{\,md}}\right]^{1/(1+md)} \tag{8}$$

$$B = \frac{16\pi v_0^{\,2}\gamma_{eff}^{\,3}}{3kT} \tag{9}$$

where m is the crystallite growth exponent, with $m = 1$ for pABA,[35] d is related to the dimensionality of crystal growth, with $d = 1$ for pABA,[35] α_{det} is the fraction of detectable crystallized volume, k_v is the crystallite growth shape factor, z is the Zeldovich factor, f_e^* is the frequency of monomer attachment to the nucleus at $\Delta\mu = 0$, c_s is the solution concentration at the crystal solution interface, d_0 is the molecular diameter $\approx (6v_o/\pi)^{1/3}$, $f_{e,s}$ is the frequency of molecular attachment per growth site at $\Delta\mu = 0$ and γ_{eff} is the effective interfacial tension.

A derivation of eq 7 is given in a previous research article.[41] $\ln\{\tau[S(S-1)^{md}]^{1/1+md}\}$ was plotted as a function of $1/T^3(\ln S)^2$ and a linear regression was fitted through the data, with the slope (SL_{lin}) equating to $\frac{16\pi v_0^{\,2}\gamma_{eff}^{\,3}}{3(1+md)k^3}$. This enabled the calculation of the effective interfacial tension. From this, the critical nucleus radius (r^*) and the number of molecules in the critical nucleus (i^*) were calculated

$$r^* = \frac{2\gamma_{eff}v_0}{kT\ln S} \tag{10}$$

$$i^* = \frac{4\pi r^{*3}}{3v_0} \tag{11}$$

Plots of $(\log S)^{-2}$ versus $\log\tau$ were constructed to determine if a nucleation mechanism change occurred during the nucleation at higher supersaturations, given that

$$\log\tau \propto \left[\frac{\gamma_{eff}^{\,3}}{T^3(\log S)^2}\right] \tag{12}$$

Large increases in the linear fit slopes would suggest a change from HEN, at lower supersaturations, to HON, at higher supersaturations.[3]

3. RESULTS AND DISCUSSION

3.1. Solubility Analysis. Small additions of H_2O to pure EtOH solutions were seen to increase pABA solubility, followed by a subsequent decrease in solubility after further addition (Figure 2). This effect has been noted in previous research performed by Rosbottom et al.[37] for pABA in mixed EtOH/nitromethane (NMe) solutions. The effect is temperature-dependent, with higher temperatures resulting in a more dramatic increase in solubility, and at lower temperatures, the increasing solubility with H_2O addition does not occur and the solubility of the system is the highest in pure EtOH.

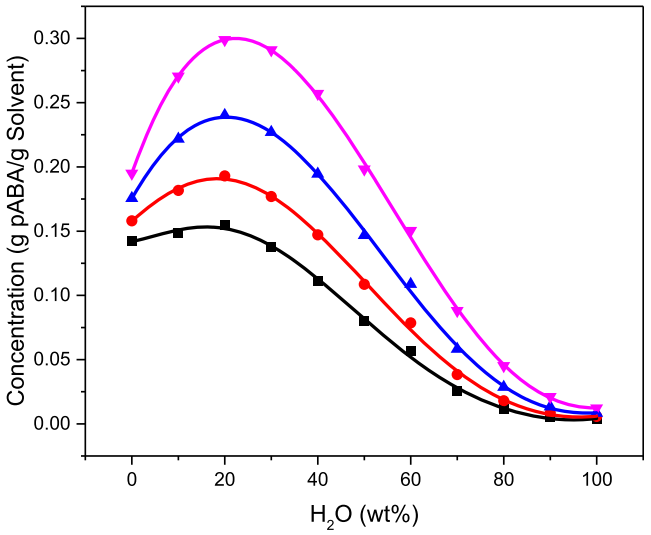

Figure 2. Solubility of pABA in EtOH/H_2O mixtures at different temperatures collected by dissolution studies. 323 K (pink ▼), 313 K (blue ▲), 303 K (red ●), and 293 K (black ■).

van't Hoff analysis provides information on the interactions between the solute and solvent molecules. In an ideal solution, the interactions are all the same, but a positive deviation from ideality indicates that solute−solvent interactions are the strongest, whereas negative deviations suggest that solute−solute interactions are the strongest and dominate the solution. Solubility data obtained for varying solution compositions (Figure 3) easily fit a linear regression model; this along with visual inspection of the crystals and no previous finding of other pABA polymorphs than the alpha form crystallizing from ethanolic solutions indicated that there was no difference in the solid-state form of pABA over the range of temperatures used.

The values of the enthalpy (ΔH_{diss}) and entropy (ΔS_{diss}) of dissolutions calculated from the slope and y-axis intercepts of the van't Hoff plots, respectively, and the linear dependence of the calculated activity coefficients (Y) on the experimentally measured molar solubility (x) are displayed in Table 1. Less than ideal behavior was observed for all pABA EtOH/H_2O solutions with values of Y for all solutions found to be above 1 over the temperature range of 283−323 K, demonstrating that the solute−solute interactions were the strongest. However, the gradient of the plots was not all found to be equal to that of the ideal solution, showing that at lower temperatures, some solutions show more than ideal behavior, although this does not occur until, for example, 274 K for the pure EtOH solution. This change was also observed for pABA solutions in a mixed EtOH/NMe solvent in a previous study.[37] It is noticeable that the solution behavior of pABA in EtOH deviates largely from those containing some/only H_2O (Figure 5b). This difference in solution behavior could be due to the different solvation energies for pABA in EtOH and H_2O.[36] The fairly comparable slopes of the mixed solvent and pure H_2O solvent solutions demonstrate that for these solutions the entropic component was changing, whereas for pure ethanolic solvent solutions, the enthalpic component was changing. The enthalpic gradient observed for the pure ethanolic solution is

DOI: 10.1021/acs.oprd.9b00242
Org. Process Res. Dev. 2019, 23, 1948−1959

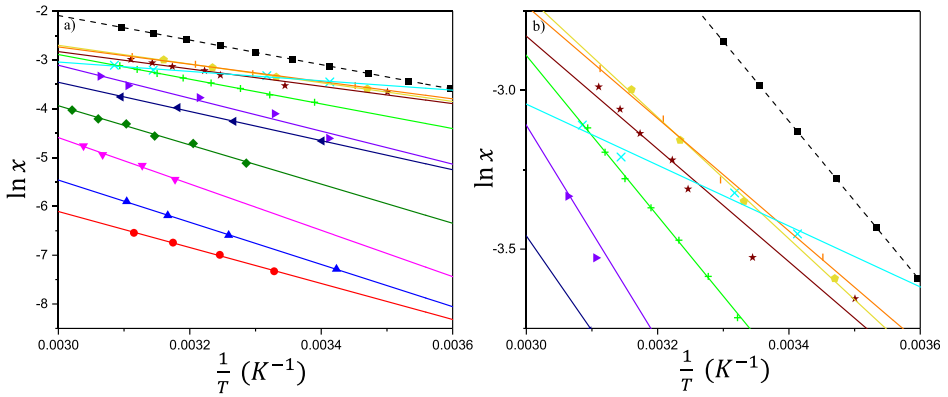

Figure 3. van't Hoff plot for pABA in EtOH/H_2O mixed solvent solutions. Dashed black line represents ideal solubility, and solid lines represent experimental solubilities for different solvent compositions: 100 wt % EtOH (blue cross), 90 wt % EtOH (brown vertical line), 80 wt % EtOH (lavender pentagon), 70 wt % EtOH (brown star), 60 wt % EtOH (green plus), 50 wt % EtOH (violet right-pointing triangle), 40 wt % EtOH (green left-pointing triangle), 30 wt % EtOH (green diamond), 20 wt % EtOH (pink down-pointing triangle), 10 wt % EtOH (blue up-pointing triangle), and 100 wt % H_2O (red circle). (a) Plots for all compositions studied. (b) Plot over a smaller range of molar solubility, showing more clearly the variation observed with EtOH solubility as a function of temperature.

Table 1. Thermodynamic Parameters Together with Linear Dependence of Y on x Derived from Solubility Analysis for Varying Compositions of pABA in EtOH/H_2O Solutions

	thermodynamic parameters		
	ΔH_{diss} (kJ mol^{-1})	ΔS_{diss} (kJ K^{-1} mol^{-1})	ln $Y = ax + b$
H_2O	−30.64	0.041	−0.32 ln x + 2.07
10:90 EtOH/H_2O	−35.93	0.062	−0.42 ln x + 1.09
20:80 EtOH/H_2O	−39.47	0.080	−0.47 ln x + 0.32
30:70 EtOH/H_2O	−33.37	0.067	−0.38 ln x + 0.35
40:60 EtOH/H_2O	−24.82	0.046	−0.16 ln x + 0.82
50:50 EtOH/H_2O	−28.06	0.058	−0.28 ln x + 0.13
60:40 EtOH/H_2O	−21.01	0.039	−0.004 ln x + 0.8
70:30 EtOH/H_2O	−14.13	0.019	0.36 ln x + 1.73
80:20 EtOH/H_2O	−15.93	0.025	0.31 ln x + 1.45
90:10 EtOH/H_2O	−14.74	0.021	0.41 ln x + 1.77
EtOH	−7.99	−0.001	1.55 ln x + 5.65

consistent with the determined solubility data, corroborating the finding that at higher temperatures, small additions of H_2O increase the solubility, whereas at lower temperatures, this effect does not occur. Turner et al.[36] calculated the values of Y for pABA in EtOH and H_2O to be 1.10 and 63.05, respectively, which correlates strongly with the calculated values here, with $61.7 < Y < 87.5$ for H_2O in the temperature range 300−321 K and $1.4 < Y < 2.1$ for EtOH in the temperature range 293−324 K, providing confidence in the reported values.

3.2. Calorimetry—Effect of Antisolvent Temperature. The addition temperature of H_2O to pABA in EtOH/H_2O mixed solvent solutions was found to have a large impact on the solution temperature, providing evidence of just how pronounced the effect of controlling antisolvent temperature can be. The amount by which the antisolvent temperature altered the solution temperature varied depending upon the amount added, with a greater volume of antisolvent having a larger impact on the solution temperature (Figure 4).

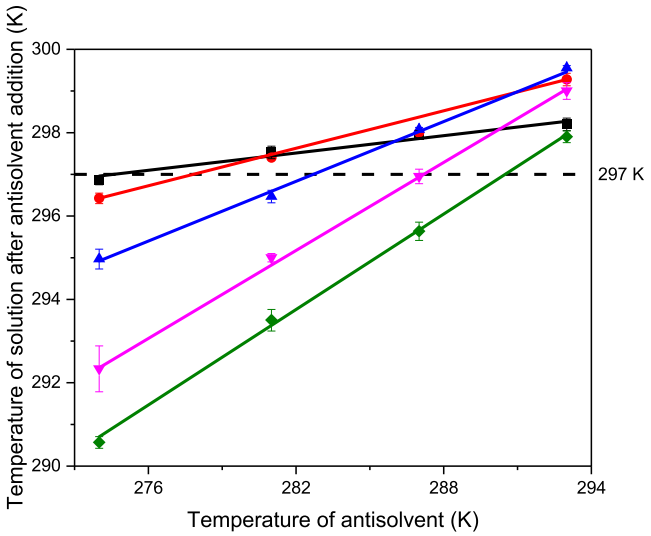

Figure 4. Effect of antisolvent temperature on solutions of pABA in the EtOH/H_2O mixed solvent held at constant temperature (297 K). Effect of antisolvent temperature on 0.2 mL initial solution (green diamond), 0.3 mL initial solution (pink down-pointing triangle), 0.5 mL initial solution (blue up-pointing triangle), 0.65 mL initial solution (red circle), and 0.8 mL initial solution (black square) shown by the gradients of the linear relationships.

A total calibration for solution volumes and temperatures was created (Figure 5) to enable the IbD approach to this study. It is worth mentioning that these calibrations are specific to this system and experimental setup, with different pieces of equipment yielding potentially different results based upon heat-transfer efficiency, mixing, etc.

Discrepancies in nucleation induction time results, obtained when the antisolvent temperature was controlled through the described methodology compared to the uncontrolled antisolvent temperature, where the antisolvent was held at the same temperature as the solution (Figure 6) were found to be large. For the controlled antisolvent temperature, the induction times were mainly much smaller than for the

DOI: 10.1021/acs.oprd.9b00242
Org. Process Res. Dev. 2019, 23, 1948−1959

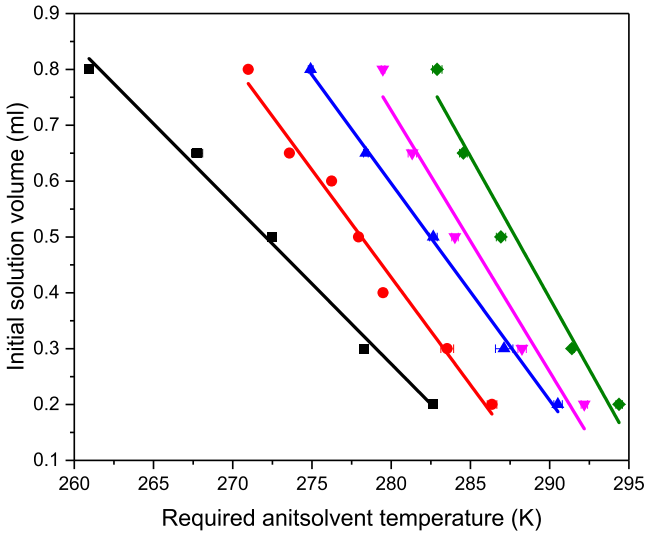

Figure 5. Antisolvent temperature calibration for the addition of water to pABA in the 70:30 wt % EtOH/H_2O solution held at set temperatures [301 K (green diamond), 299 K (pink down-pointing triangle), 297 K (blue up-pointing triangle), 295 K (red circle), and 293 K (black square)] in order to maintain solution temperatures. The temperature of the antisolvent is plotted against the initial amount of solution used.

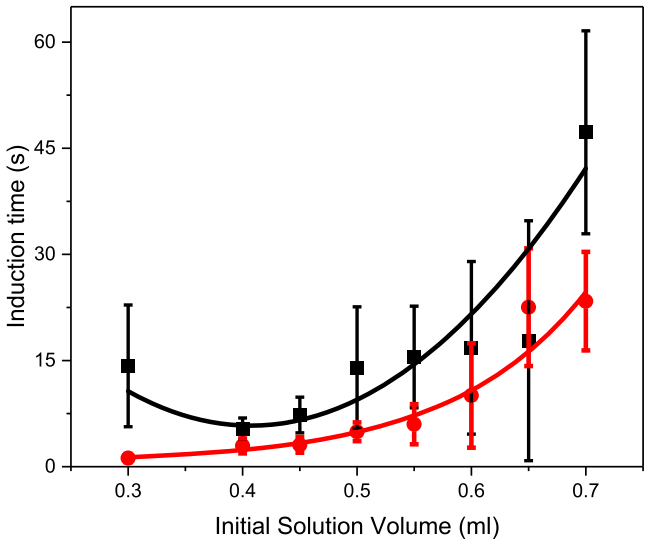

Figure 6. Difference in induction time measurements for uncontrolled (black square) and controlled (red circle) antisolvent temperature addition for a solution temperature of 295 K. Error bars show standard deviation of repeats. Trend lines fitted for both data sets to highlight deviation.

experiments performed without control, which can be attributed to the heat of mixing increasing the solution temperature for uncontrolled experiments and as such decreasing the supersaturation, before subsequent slow and uncontrolled cooling to the solution set temperature as the experimental system reequilibrated the solution temperature. Furthermore, the standard deviations of the controlled experiments were much lower than that of the uncontrolled experiments. This was due to the IbD approach in the controlled experiments, indicating that deviations in results were due to the stochasticity of nucleation as opposed to the added effect of temperature variations, which was a component of the uncontrolled experiments.

It is noticeable that lower initial solution volumes have a lower standard deviation than higher initial solution volumes. This is due to the higher initial solution volumes generating a lower supersaturation, as less antisolvent was added, and as such, this lower driving force generates more variation in the stochasticity of nucleation. This will be discussed in more detail in the next section.

3.3. Compositions, Concentrations, and Supersaturations. The experimental methodology applied to accelerating nucleation was able to cover a wide range of solution compositions from 11 to 53 wt % EtOH, concentrations from 22.4 to 104.3 g pABA kg^{-1} solvent, and supersaturations from 1.08 to 4.73 (Table 2). It is important to note that other systems studied through this methodology could achieve different and potentially greater variations in compositions and concentrations, as well as higher supersaturations, which will be discussed in Section 4.2 of this article.

An overall nonlinear decreasing trend of τ with increasing supersaturation and hence an increased rate of nucleation (Figure 7), for pABA crystallizing from EtOH/H_2O mixtures, were observed. At high solution supersaturations, changes in τ were smaller than at lower supersaturations, where even small changes in S had a pronounced effect on induction times.

At relatively low supersaturations, high standard deviations in induction time results were observed. This stochasticity and lack of reproducibility of induction time measurements at low S have led to the use of probability distribution functions in induction time studies to determine nucleation parameters,[42] indicating that a very large number of repeats are needed for each supersaturation used. However, because of supersaturation being the driving force for crystal nucleation, it was seen that at the higher supersaturations and lower induction times, where the stochastic nature of nucleation is slightly overcome, the results were more reproducible, with less deviation from one experiment to the next (Figure 8).

For all concentrations and compositions used, it is noticeable that the change in induction times using the proposed method was substantial, with changes from periods of hours to seconds (Figure 7b). Furthermore, it provides significant information regarding when crystallization would occur at different supersaturations, indicating that great control could be achieved over the process of pABA crystallizing from EtOH/H_2O solutions. This "control" could be of considerable impact to systems that are required to remain uncrystallized for a certain duration of time or conversely need to crystallize at a specific time, such as diesel fuel, agrochemical products, pharmaceutical supersaturated dosage forms, and so forth.

Furthermore, high supersaturations were achieved at a very fast rate under this "instant addition" methodology unlike other crystallization methodologies to produce high supersaturations, such as crash cooling, which can take minutes to reach a desired level of supersaturation[43] and, as such, can be subject to unwanted crystallization before the level is reached. This was very important for the higher supersaturation experiments performed as the induction times themselves were only one or more seconds, indicating that other methodologies might not have been able to produce such a supersaturation level for the system of study, such as conventional cooling crystallization, evaporative crystallization, isothermal crystallization, and so forth. For example, for pABA in EtOH, in order to achieve S = 2 at 293 K, a saturation

DOI: 10.1021/acs.oprd.9b00242
Org. Process Res. Dev. 2019, 23, 1948−1959

Table 2. Solution Compositions, Concentrations, and Supersaturations over the Range of Initial Solution Volumes Selected[a]

initial solution volume (mL)	final solution H_2O content (wt %)	final solution EtOH content (wt %)	final solution concentration (g pABA kg^{-1} solution)	supersaturation at solution temperature of 293 K	supersaturation at solution temperature of 295 K	supersaturation at solution temperature of 297 K	supersaturation at solution temperature of 299 K	supersaturation at solution temperature of 301 K
0.8	47	53	104.3	Fr	1.08	nc	nc	nc
0.75	51	49	96.5	Fr	1.15	1.09	nc	nc
0.7	55	45	88.9	Fr	1.25	1.17	1.10	nc
0.65	59	41	81.4	Fr	1.37	1.28	1.20	1.12
0.6	62	38	74.2	Fr	1.51	1.41	1.32	1.23
0.55	66	34	67.2	1.82	1.69	1.57	1.46	1.36
0.5	69	31	60.3	2.06	1.91	1.77	1.64	1.52
0.45	73	27	53.6	2.36	2.18	2.01	1.86	1.72
0.4	76	24	47.0	2.72	2.51	2.31	2.12	1.96
0.35	79	21	40.7	3.16	2.90	2.66	2.44	2.24
0.3	83	17	34.4	3.68	3.36	3.07	2.80	2.55
0.25	86	14	28.4	4.25(lv)	3.85(lv)	3.49(lv)	3.16(lv)	2.86(lv)
0.2	89	11	22.4	4.73(lv)	4.23(lv)	3.79(lv)	3.40(lv)	3.06(lv)

[a]"fr" denotes solutions where the required antisolvent temperature to maintain the solution temperature was too low and would cause the water antisolvent to freeze. "nc" denotes solutions that would not crystallize because of too low supersaturations. "lv" denotes solutions that underwent the described experimental procedure but where the solution volume was too low for accurate induction time detection. "Final solution" refers to the solution after antisolvent addition.

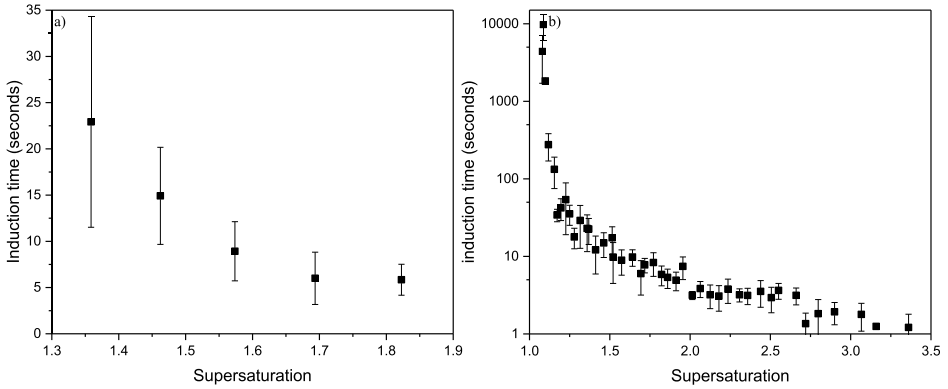

Figure 7. Induction time vs supersaturation for pABA in EtOH/H_2O mixture solutions, with error bars showing standard deviation of 16 repeats for each data point. (a) Data obtained at a final solution concentration of the 67.2 g pABA kg^{-1} solvent mixture at all temperatures and (b) all concentrations and compositions at all temperatures (log scale used for the *y*-axis).

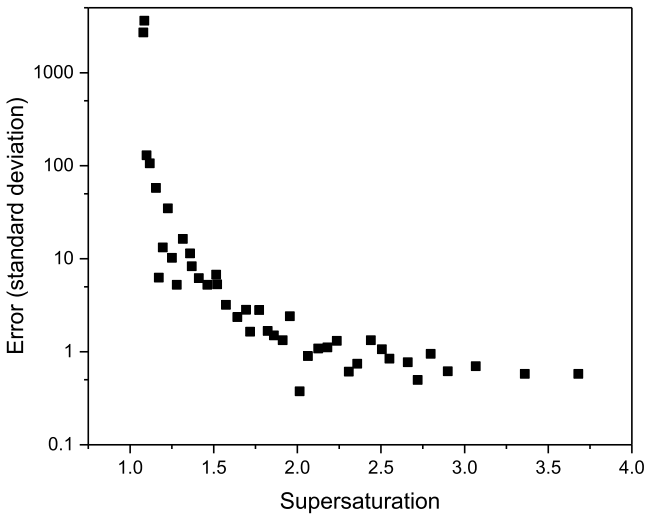

Figure 8. Change in standard deviation of induction time measurements, over 16 repeats, as a function of supersaturation.

temperature of 359 K was required, which is above the boiling point of EtOH, indicating that normal isothermal approaches are not feasible, providing further evidence of the benefits of this IbD antisolvent approach to achieving high supersaturations.

An alternative explanation to how induction times were reduced substantially under the proposed IbD methodology is that "cold spots" were created upon addition of the colder antisolvent to the higher temperature solution, creating areas of localized high supersaturations. However, given that the mixing times would be short in comparison to the induction times, even at higher solution supersaturations, this is not likely to be the case. High supersaturations and low induction times were achieved by direct mixing of the antisolvent with the solution and subsequent homogeneity of solution temperature in a very short time period before subsequent nucleation. Nevertheless, at larger scales, such as industrial scales, this could be a problem because of difficulties in mixing and temperature regulation.[31,34] This will be discussed further in Section 4.3.

A comparative method to IbD outlined here is combined cooling and antisolvent crystallization (CCAC),[29] which

DOI: 10.1021/acs.oprd.9b00242
Org. Process Res. Dev. 2019, 23, 1948−1959

Table 3. Kinetic Parameters, γ_{eff}, r^*, and i^*, Calculated from Antisolvent Induction Time Experiments as a function of Solution Concentration and Composition over a Range of Supersaturations

final solution concentration (g kg^{-1})	EtOH/H_2O solvent ratio (wt %)	temperature range (K)	γ_{eff} (mJ m^{-2})	supersaturation range	r^* (nm)	i^* (molecules)
34.4	17:83	293−301	8.39	3.7−2.6	0.53−0.71	4−9
40.7	21:79	293−301	7.86	3.2−2.2	0.56−0.78	4−12
47.0	24:76	293−301	6.39	2.7−2.0	0.52−0.76	4−11
53.6	27:73	293−301	5.29	2.4−1.7	0.50−0.78	3−12
60.3	31:69	293−301	4.50	2.1−1.5	0.51−0.85	3−16
67.2	34:66	293−301	3.35	1.8−1.4	0.46−0.87	2−17
74.2	38:62	295−301	2.77	1.5−1.2	0.54−0.1.08	4−32
81.4	41:59	295−301	2.11	1.4−1.1	0.55−1.51	4−87
88.9	45:55	295−299	2.32	1.3−1.1	0.84−1.98	15−196

utilizes a polythermal cooling crystallization methodology with a controlled addition of antisolvent to achieve high supersaturations. The advantages of IbD over CCAC are twofold: IbD is simpler compared to CCAC, with just control of antisolvent temperature being prevalent as opposed to trying to control the cooling rate, enthalpies of mixing, and antisolvent addition rate, all at once. Also, IbD utilizes direct mixing to maintain the solution temperature, whereas CCAC utilizes conduction cooling from a reactor jacket, which can cause difficulties in solution homogeneity at larger industrial scales, as discussed in the Introduction section.

3.4. Nucleation Kinetics Analysis. Induction time (τ) data were collected as a function of supersaturation (S) for a range of concentrations and compositions of pABA in EtOH/H_2O mixed solutions. The data collected were used to calculate interfacial tensions (γ_{eff}) for solution concentrations between 88.9 and 34.4 pABA kg^{-1} solvent mixture using eq 7 and the slope from the linear relationship (SL_{lin}), equal to $\frac{16\pi v_0^2 \gamma_{eff}^3}{3(1+md)k^3}$. Example plots of the linear relationship are given in Supporting Information S7. Calculated values of γ_{eff}, r^*, and i^* for the range of concentrations and compositions used are displayed in Table 3.

3.4.1. Effective Interfacial Tension. Calculated γ_{eff} values showed a marked decrease as the supersaturation and H_2O content decreased. The compositional effect on γ_{eff} correlates with the solubility of the system, with a lower solubility attributed to a higher γ_{eff}.[44] Furthermore, a higher rate of decrease in γ_{eff} was observed for higher H_2O contents, with the rate decreasing along with the H_2O content, showing a similar trend to induction time results. This result provides evidence that it may be possible to extrapolate γ_{eff} values over the compositional range, even to the single solvent system boundaries; however, further work is clearly needed to probe this possibility.

Sullivan et al.[45] and Toroz et al.[35] recently reported values of γ_{eff} for pABA in acetonitrile, 2-propanol, ethyl acetate, and ethanol, respectively, using isothermal experimental methodologies, in the range of 1.33−2.44 mJ m^{-2} over $1.08 < S < 1.35$ and 0.85−1.31 mJ m^{-2} over the smaller range of $1.04 < S < 1.15$, respectively. The calculated values of Sullivan et al. compare well with those calculated in a similar supersaturation range in this study, providing confidence in the results obtained. However, these studies were concerned with single solvent systems, and to the authors' knowledge, no current open literature source provides details of values of γ_{eff} for EtOH/H_2O mixed systems. Jiang and Ter Horst[42] previously studied a similar compound in a similar solvent system, *m*-aminobenzoic acid in mixed EtOH/H_2O solution, and determined the value of γ_{eff} for this system to be 8.7 mJ m^{-2}, which correlates well with the higher γ_{eff} values calculated in this study.

Interestingly, although it has been previously found that for pABA in EtOH solutions a lower pABA concentration correlates to lower values of γ_{eff},[35] the same trend was not followed for these results. Instead, the opposite occurs, with a lower concentration correlating to a higher γ_{eff}. This result suggests that either the supersaturation or the compositional effects dominate γ_{eff}, although it is not possible to disentangle these factors under this experimental procedure because of the supersaturation and composition being intrinsically linked.

Furthermore, induction time data over single temperatures, that is, multiple compositions, was studied. Figure 9 displays

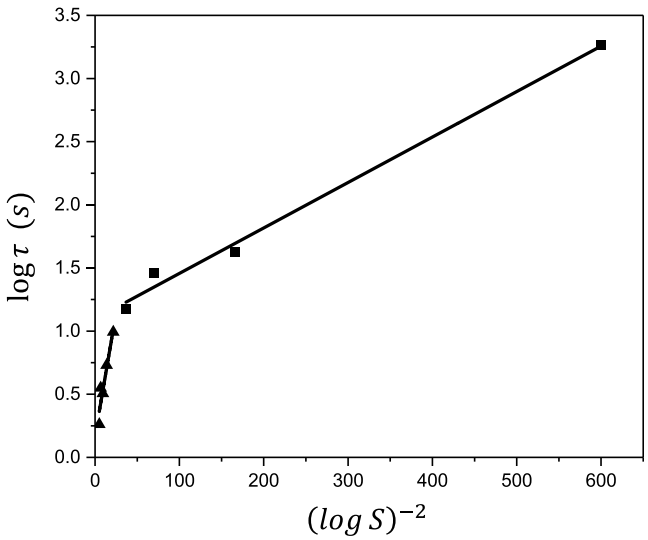

Figure 9. Induction time vs supersaturation for single temperature and multiple composition solutions of pABA in EtOH/H_2O mixtures for solutions at 299 K.

data collected for a single temperature of 299 K. For temperatures of 295−301 K, there were two linear relationships found for the experimental data, showing two distinct slopes. This is indicative of a mechanistic change in the nucleation of pABA from the mixed solvent system, changing from HEN to HON as the supersaturation reached a sufficient level. This finding has been observed in a number of research studies with critical supersaturations attributed to this mechanistic change being varied depending upon the system of study. Kim and Kim[12] found the HEN to HON critical

DOI: 10.1021/acs.oprd.9b00242
Org. Process Res. Dev. 2019, 23, 1948−1959

supersaturation level of S = 1.7 for the aqueous sodium chloride solution using methanol as an antisolvent, whereas Söhnel and Mullin[46] found S = 20 for reaction crystallization of calcium carbonate from the aqueous sodium carbonate solution. In the case of pABA in EtOH/H_2O solutions in this study, the change occurred at $S \approx 1.5$.

This slope change was not observed at the set temperature of 293 K, which is due to the lowest level of supersaturation achieved being above the $S \approx 1.5$ threshold.

3.4.2. Critical Nucleus Radius and Number of Molecules in the Critical Nucleus. Values of r^* and i^* both showed a similar trend to the obtained induction time measurements as a function of supersaturation for pABA in EtOH/H_2O mixed solutions, that is, lower values correlate with higher supersaturations (Figure 10), which is a trend previously observed

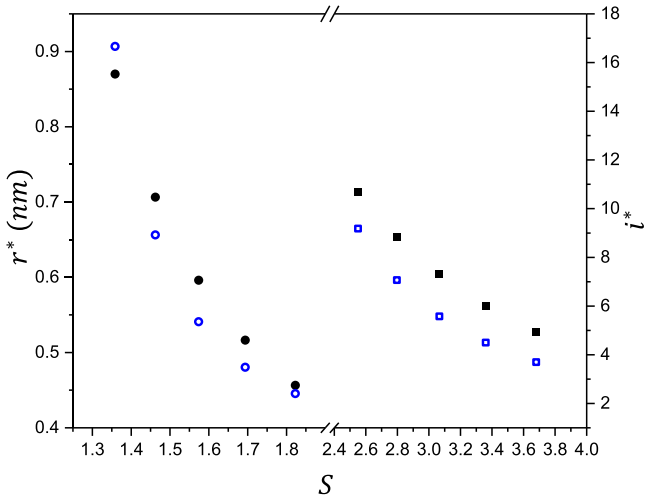

Figure 10. r^* (solid objects) and i^* (hollow objects) vs supersaturation from the data obtained at a final solution concentration of 34.4 g pABA kg^{-1} solvent mixture (black ■/blue □) and a final solution concentration of 67.2 g pABA kg^{-1} solvent mixture (black ●/blue ○). Break applied to graph between 1.9 and 2.4.

with pABA in ethanolic solutions[35] and is expected with the supersaturation dependence (eqs 10 and 11). Additionally, the nonlinear trend is also consistent with smaller changes in values observed at higher supersaturations and larger variation achieved at lower supersaturations. However, a higher supersaturation did not solely dictate r^* and i^*, as lower values of r^* and i^* were determined at lower supersaturations in some cases. This is compositional dependency, as the values of γ_{eff} varied with the solubility of the systems studied, as described previously. This indicates that although supersaturation has a strong effect on the size of the critical nucleus, the composition has a larger effect because of the γ_{eff} associated with the formation of a critical nucleus.

Values of i^* as low as 2 and 3 were calculated for this system at relatively high supersaturations and at certain compositions. In a previous study by this research group,[35] it was determined through small-angle X-ray studies that stable dimers are formed in equilibrium with pABA in the EtOH solution, which is suggestive that i^* should be larger than 2, otherwise critical nuclei would exist in an undersaturated state. Nevertheless, this is suggestive of a nonclassical nucleation route, and as such, the use of CNT, as the analysis methodology in this study, can determine that i^* = 2. Furthermore, in the previously highlighted study, an isothermal methodology was also used to determine key nucleation parameters and calculated i^* values as low as 3 using CNT at lower supersaturations than were achieved in this current study, giving confidence in the results obtained here under a CNT methodology.

4. CONCLUSIONS

4.1. Conclusions of This Study. Overall, a comprehensive experimental investigation was made, introducing a simple methodology to accelerate crystal nucleation and enable key kinetic parameters to be determined, which would otherwise be unachievable through conventional crystallization methods, while also providing a possibility for a future predictive ability of the nucleation of slowly nucleating systems.

A route to the accelerated nucleation of pABA in ethanol/water (EtOH/H_2O) mixed solvent solutions, using antisolvent crystallization, was presented using an "isothermal by design" approach. Supersaturations that were accessible through the IbD methodology of this system were higher than could be achieved through traditional crystallization methods, achieving $S > 4$. Initial solubility studies determined that small additions of H_2O to pABA in EtOH solutions increased the solubility, but further additions decreased the solubility. All solutions of pABA in the EtOH/H_2O mixed solvent solution were less than ideal.

The enthalpy of mixing upon addition of H_2O as an antisolvent had a dramatic effect on the solution temperature and as such the induction time results. Control of antisolvent addition temperature, through calorimetry calibrations, ensured that the IbD experiments provided the relevant information for accurate and comparable nucleation kinetic analysis. Induction times were controlled with ease, with significant changes from solutions at low supersaturations and high supersaturations by 4 orders of magnitude. The high driving force to nucleation for solutions at high supersaturations reduced the standard deviation of induction time results when compared to that at low supersaturation conditions.

Nucleation kinetics of a range of solution compositions and concentrations were determined from the obtained experimental data. Values of γ_{eff} decreased with decreasing supersaturation and H_2O content and increasing concentration. The observed nonlinear trend of changing γ_{eff} with composition was similar to that observed for induction time measurements. A change of nucleation mechanism from HEN to HON was found as the supersaturation was increased to a critical value of around 1.5. Values of r^* and i^* both showed an expected trend with respect to an increased supersaturation being met with smaller critical nucleus sizes. However, the results demonstrated that r^* and i^* were also compositionally dependent, with supersaturation not solely determining the critical nucleus size, showing that solubility plays a large role in the nucleation kinetics of pABA crystallizing from ethanol/water mixtures.

4.2. Future Work and Current Limitations. This study has detailed a useful and novel methodology for determining key nucleation parameters more effectively over a vast range of supersaturations. However, it is currently subject to certain limitations and could be improved further.

One limitation of using the current system is the previously highlighted solubility of pABA in mixed EtOH/H_2O solvents. This is due to an increased pABA solubility upon small additions of H_2O to EtOH solvent, limiting compositions accessible to solely increase supersaturations, limiting the

DOI: 10.1021/acs.oprd.9b00242
Org. Process Res. Dev. 2019, 23, 1948−1959

supersaturations that could be achieved in the allowable working solution volume of the experimental apparatus used. Many other systems would not be subject to this limitation however, such as α-lactose in isopropanol/water and acetone/water mixtures.[47]

Another limitation is that in order to use the IbD methodology for accelerated nucleation studies, a "reasonable" solubility is required for the initial solvent with the second solvent having a much lower solubility, as highlighted in the workflow given in Figure 1. However, this could easily be mitigated by continuous crystallization IbD methodologies, where the issue of solubility would be negated by the low volumes mixed at one instance, such as use with T-mixer geometries.[12]

Furthermore, supersaturations were limited under this system of study as a minimum detection time of 1 s was applicable for the experimental apparatus used. Therefore, if different apparatus and/or process analytical techniques (PAT) were used, then resolution of results could be improved. Nevertheless, systems that nucleate slower than the one in this study would not be affected by this limitation, and detection could be more accurate.

Induction time data can be dependent upon the stochastic nature of nucleation and as such can be affected by relatively high standard deviations of repeats, as discussed in Section 3.3. This indicates that crystallization parameters calculated from induction data can be subject to some variability. Further use of PAT to determine the point of detectable nucleation more accurately, such as use of complimentary Fourier transform infrared spectroscopy,[48] UV/vis,[49] microscopy,[50] and so forth, could ensure that key crystallization parameters are calculated more accurately; however, at the scales used for the current study (1 mL) and the experimental apparatus, these parameters are not applicable.

The calculated values of γ_{eff} showed a trend in decreasing value alongside a decrease in H_2O solvent content. This trend needs to be further studied to understand if it is possible to extrapolate calculated values of γ_{eff} to various other solvent compositions. Furthermore, a statistical analysis of results could provide an avenue in which to model the effect of supersaturation on induction time as well as the standard deviations associated with the induction time measurements.

4.3. Potential for Transferring IbD Methodology to Industrial Scales. The methodology outlined in this study would be useful in an industrial R&D environment, enabling key crystallization parameters to be determined more accurately prior to large operation, aiding in improved large-scale operation and greater control of product performance, particularly with respect to the physical stability of materials, such as undiscovered polymorphs. Furthermore, current tests to predict nucleation events of slowly nucleating systems involve large timescales for experiments, which hinder the progression of products to manufacture and market. This methodology would speed up this step and enable a product to get to market quicker.

Also, the methodology provides clarity on the large effect that antisolvent addition can have upon otherwise well-controlled solution conditions, which, given the larger volumes used at industrial scales, can be even more problematic. This important aspect of the methodology highlights the fact that the antisolvent temperature must be offset in comparison to the solution temperature in order to ensure as accurate solution conditions as possible and, as such, greater product control, regardless of scale or industry application.

Nevertheless, the addition of antisolvent at controlled temperatures did cause slight heating/cooling effects to the "isothermal" solution, but as described previously, this was negligible and quick to return to the solution temperature at the scale studied. However, at larger scales, this could be more problematic and a longer time period to return to the set solution temperature could occur. This could be controlled through very accurate antisolvent addition calorimetry calibrations, but it should be noted that this slight effect is much smaller than would occur without the IbD methodology in place.

Furthermore, issues with cold spots, as alluded to previously, and inhomogeneous mixing at industrial scales could be problematic with the IbD methodology outlined. However, these issues can be overcome with appropriate internals to ensure that homogeneous solutions are formed, which could be achieved through baffles, correct internals material choice, and rotation speed.[32,33] Also, manipulation of antisolvent addition technique, such as an antisolvent distributor or sparging, which is currently under research, could overcome these issues. Furthermore, if this methodology is utilized with gas antisolvent (GAS), then issues with mixing would be negligible.[51] This could also be negated by continuous crystallization processes,[52,53] where mixing can be extremely rapid in a much smaller volume.

■ ASSOCIATED CONTENT

Supporting Information

The Supporting Information is available free of charge on the ACS Publications website at DOI: 10.1021/acs.oprd.9b00242.

Crystallization; free energy schematic for nucleation; Technobis Crystal 16 system; transmission profiles as a function of time; temperature calibration for the Technobis Crystal 16® system; solubility determination and data; antisolvent temperature calibrations; isothermal analysis; nucleation mechanism change; and critical nucleus (PDF)

■ AUTHOR INFORMATION

Corresponding Author

*E-mail: k.j.roberts@leeds.ac.uk.

ORCID

Peter L. Kaskiewicz: 0000-0001-6708-6687
Xiaojun Lai: 0000-0002-4934-511X
Nicholas J. Warren: 0000-0002-8298-1417
Kevin J. Roberts: 0000-0002-1070-7435

Notes

The authors declare no competing financial interest.

■ ACKNOWLEDGMENTS

This research was carried out at the EPSRC Centre for Doctoral Training in Complex Particulate Products and Processes (EP/L015285/1) and forms part of the doctoral studies of one of us (P.L.K.) in collaboration with Infineum UK Ltd and Syngenta UK Ltd, who we gratefully acknowledge for their support of this work. We also acknowledge the EPSRC (EP/IO14446/1 and EP/IO13563/1) for support of crystallization research at the University of Leeds.

DOI: 10.1021/acs.oprd.9b00242
Org. Process Res. Dev. 2019, 23, 1948−1959

NOMENCLATURE

A, pre-exponential factor
c, absolute solute concentration (m^{-3})
c^*, saturation concentration (m^{-3})
c_s, solution concentration at the crystal solution interface (m^{-3})
d, dimensionality of crystal growth
d_0, molecular diameter (m)
f_e^*, frequency of monomer attachment to the nucleus at $\Delta\mu = 0$ ($1\ s^{-1}$)
$f_{e,s}$, frequency of molecular attachment per growth site at $\Delta\mu = 0$ ($1\ s^{-1}$)
i^*, number of molecules in the critical nucleus
J, rate of nucleation ($1\ m^{-3}\ s^{-1}$)
k, Boltzmann constant ($J\ K^{-1}$)
k_v, crystallite growth shape factor
m, crystallite growth exponent
q, heating/cooling rate ($K\ min^{-1}$)
R, ideal gas constant ($J\ mol^{-1}\ K^{-1}$)
r, nucleus radius (m)
r^*, critical nucleus radius (m)
S, supersaturation
T, temperature (K)
T_c, crystallization temperature (K)
$T_{c,l}$, crystallization temperatures at the kinetic limit (K)
T_{diss}, dissolution temperature (K)
T_e, equilibrium saturation temperatures (K)
v_0, volume occupied by a solute molecule in a crystal (m^3)
x, molar solubility
x_{ideal}, ideal molar solubility
z, Zeldovich factor
α_{det}, fraction of detectable crystallized volume
ΔG, Gibbs free energy ($kJ\ mol^{-1}$)
ΔH_{diss}, enthalpy of dissolution ($kJ\ mol^{-1}$)
ΔS_{diss}, entropy of dissolution ($kJ\ K^{-1}\ mol^{-1}$)
Y, activity coefficient
γ, interfacial tension ($mJ\ m^{-2}$)
γ_{eff}, effective interfacial tension ($mJ\ m^{-2}$)
τ, induction time (s)

REFERENCES

(1) Khan, S.; Ma, C. Y.; Mahmud, T.; Penchev, R. Y.; Roberts, K. J.; Morris, J.; Özkan, L.; White, G.; Grieve, B.; Hall, A.; Buser, P.; Gibson, N.; Keller, P.; Shuttleworth, P.; Price, C. J. In-Process Monitoring and Control of Supersaturation in Seeded Batch Cooling Crystallisation ofl-Glutamic Acid: From Laboratory to Industrial Pilot Plant. *Org. Process Res. Dev.* **2011**, *15*, 540−555.

(2) Camacho Corzo, D.; Ma, C.; Ramachandran, V.; Mahmud, T.; Roberts, K. Crystallisation Route Map. In *Engineering Crystallography: From Molecule to Crystal to Functional Form*; Roberts, K., Docherty, R., Tamura, R., Eds.; Springer Science + Business Media, 2017; pp 179−213.

(3) Mullin, J. W. *Crystallization*, 4th ed.; Butterworth-Heinemann: Oxford, 2001.

(4) Kashchiev, D. *Nucleation*; Butterworth-Heinemann: Oxford, 2000.

(5) Kwokal, A. Preparation, Stabilisation and Advantages of Metastable Polymorphs. In *Engineering Crystallography: From Molecule to Crystal to Functional Form*; Roberts, K. ., Docherty, R., Tamura, R., Eds.; Springer Science + Business Media, 2017; pp 247−260.

(6) Groen, H.; Roberts, K. J. Nucleation, Growth, and Pseudo-Polymorphic Behavior of Citric Acid as Monitored in Situ by Attenuated Total Reflection Fourier Transform Infrared Spectroscopy. *J. Phys. Chem. B* **2001**, *105*, 10723−10730.

(7) MacMillan, S. D.; Roberts, K. J.; Rossi, A.; Wells, M. A.; Polgreen, M. C.; Smith, I. H. In Situ Small Angle X-Ray Scattering (SAXS) Studies of Polymorphism with the Associated Crystallization of Cocoa Butter Fat Using Shearing Conditions. *Crystal Growth Des.* **2002**, *2*, 221−226.

(8) Bauer, J.; Spanton, S.; Henry, R.; Quick, J.; Dziki, W.; Porter, W.; Morris, J. Ritonavir: An Extraordinary Case of Conformational Polymorphism. *Pharm. Res.* **2001**, *18*, 859−866.

(9) Heffernan, C.; Ukrainczyk, M.; Zeglinski, J.; Hodnett, B. K.; Rasmuson, Å. C. Influence of Structurally Related Impurities on the Crystal Nucleation of Curcumin. *Crystal Growth Des.* **2018**, *18*, 4715−4723.

(10) McAfee, D. A.; Hadgraft, J.; Lane, M. E. Rotigotine: The First New Chemical Entity for Transdermal Drug Delivery. *Eur. J. Pharm. Biopharm.* **2014**, *88*, 586−593.

(11) Bajaj, S.; Singla, D.; Sakhuja, N. Stability Testing of Pharmaceutical Products. *J. Appl. Pharm. Sci.* **2012**, *2*, 129−138.

(12) Kim, K.-J.; Kim, J.-K. Nucleation and Supersaturation in Drowning-out Crystallization Using a T-Mixer. *Chem. Eng. Technol.* **2006**, *29*, 951−956.

(13) Pina, C. M.; Fernández-Díaz, L.; Prieto, M.; Veintemillas-Verdaguer, S. Metastability in drowning-out crystallisation: precipitation of highly soluble sulphates. *J. Cryst. Growth* **2001**, *222*, 317−327.

(14) Croker, D. M.; Kelly, D. M.; Horgan, D. E.; Hodnett, B. K.; Lawrence, S. E.; Moynihan, H. A.; Rasmuson, Å. C. Demonstrating the Influence of Solvent Choice and Crystallization Conditions on Phenacetin Crystal Habit and Particle Size Distribution. *Org. Process Res. Dev.* **2015**, *19*, 1826−1836.

(15) Musumeci, D.; Hunter, C. A.; McCabe, J. F. Solvent Effects on Acridine Polymorphism. *Crystal Growth Des.* **2010**, *10*, 1661−1664.

(16) Kordylla, A.; Koch, S.; Tumakaka, F.; Schembecker, G. Towards an Optimized Crystallization with Ultrasound: Effect of Solvent Properties and Ultrasonic Process Parameters. *J. Cryst. Growth* **2008**, *310*, 4177−4184.

(17) Lyczko, N.; Espitalier, F.; Louisnard, O.; Schwartzentruber, J. Effect of Ultrasound on the Induction Time and the Metastable Zone Widths of Potassium Sulphate. *Chem. Eng. J.* **2002**, *86*, 233−241.

(18) Bari, A. H.; Chawla, A.; Pandit, A. B. Sono-crystallization kinetics of K 2 SO 4 : Estimation of nucleation, growth, breakage and agglomeration kinetics. *Ultrason. Sonochem.* **2017**, *35*, 196−203.

(19) Kleetz, T.; Funke, F.; Sunderhaus, A.; Schembecker, G.; Wohlgemuth, K. Influence of Gassing Crystallization Parameters on Induction Time and Crystal Size Distribution. *Crystal Growth Des.* **2016**, *16*, 6797−6803.

(20) Wohlgemuth, K. *Induced Nucleation Processes during Batch Cooling Crystallization*, Ph.D. Thesis, TU Dortmund University: Dortmund, 2012.

(21) Curcio, E.; López-Mejías, V.; Di Profio, G.; Fontananova, E.; Drioli, E.; Trout, B. L.; Myerson, A. S. Regulating Nucleation Kinetics through Molecular Interactions at the Polymer-Solute Interface. *Crystal Growth Des.* **2014**, *14*, 678−686.

(22) Diao, Y.; Myerson, A. S.; Hatton, T. A.; Trout, B. L. Surface Design for Controlled Crystallization: The Role of Surface Chemistry and Nanoscale Pores in Heterogeneous Nucleation. *Langmuir* **2011**, *27*, 5324−5334.

(23) Wijethunga, T. K.; Baftizadeh, F.; Stojaković, J.; Myerson, A. S.; Trout, B. L. Experimental and Mechanistic Study of the Heterogeneous Nucleation and Epitaxy of Acetaminophen with Biocompatible Crystalline Substrates. *Crystal Growth Des.* **2017**, *17*, 3783−3795.

(24) Sangwal, K.; Mielniczek-Brzóska, E. Antisolvent Crystallization of Aqueous Ammonium Dihydrogen Phosphate Solutions by Addition of Methanol. *J. Cryst. Growth* **2016**, *451*, 139−149.

(25) Granberg, R. A.; Bloch, D. G.; Rasmuson, Å. C. Crystallization of paracetamol in acetone-water mixtures. *J. Cryst. Growth* **1999**, *198−199*, 1287−1293.

(26) Roelands, C. P. M.; Jiang, S.; Kitamura, M.; Ter Horst, J. H.; Kramer, H. J. M.; Jansens, P. J. Antisolvent Crystallization of the

DOI: 10.1021/acs.oprd.9b00242
Org. Process Res. Dev. 2019, 23, 1948−1959

Polymorphs ofl-Histidine as a Function of Supersaturation Ratio and of Solvent Composition. *Crystal Growth Des.* **2006**, *6*, 955−963.
(27) Hermanto, M. W.; Chow, P. S.; Tan, R. B. H. Operating Strategy to Produce Consistent CSD in Combined Antisolvent-Cooling Crystallization Using FBRM. *Ind. Eng. Chem. Res.* **2012**, *51*, 13773−13783.
(28) Sheikhzadeh, M.; Trifkovic, M.; Rohani, S. Adaptive MIMO Neuro-Fuzzy Logic Control of a Seeded and an Unseeded Anti-Solvent Semi-Batch Crystallizer. *Chem. Eng. Sci.* **2008**, *63*, 1261−1272.
(29) Lindenberg, C.; Krättli, M.; Cornel, J.; Mazzotti, M.; Brozio, J. Design and Optimization of a Combined Cooling/Antisolvent Crystallization Process. *Cryst. Growth Des.* **2009**, *9*, 1124−1136.
(30) Yang, Y.; Nagy, Z. K. Combined Cooling and Antisolvent Crystallization in Continuous Mixed Suspension, Mixed Product Removal Cascade Crystallizers: Steady-State and Startup Optimization. *Ind. Eng. Chem. Res.* **2015**, *54*, 5673−5682.
(31) Bentham, E. J.; Heggs, P. J.; Mahmud, T. CFD Modelling of Conjugate Heat Transfer in a Pilot-Scale Unbaffled Stirred Tank Reactor with a Plain Jacket. *Can. J. Chem. Eng.* **2019**, *97*, 573−585.
(32) Liang, K.; White, G.; Wilkinson, D.; Ford, L. J.; Roberts, K. J.; Wood, W. M. L. An Examination into the Effect of Stirrer Material and Agitation Rate on the Nucleation ofl-Glutamic Acid Batch Crystallized from Supersaturated Aqueous Solutions. *Crystal Growth Des.* **2004**, *4*, 1039−1044.
(33) Liang, K.; White, G.; Wilkinson, D.; Ford, L. J.; Roberts, K. J.; Wood, W. M. L. Examination of the Process Scale Dependence ofl-Glutamic Acid Batch Crystallized from Supersaturated Aqueous Solutions in Relation to Reactor Hydrodynamics. *Ind. Eng. Chem. Res.* **2004**, *43*, 1227−1234.
(34) Al-Marri, M.; Mahmud, T.; Roberts, K. J. A Flexible Heat Transfer Model for Simulating the Performance of Batch Cooling Crystallization as a Function of Process Scale Size. In *Proceedings of the 17th International Symposium on Industrial Crystallization*; Ulrich, J., Jansens, P., Roelands, M., Eds., 2008; Vol. 2, pp 613−620.
(35) Toroz, D.; Rosbottom, I.; Turner, T. D.; Corzo, D. M. C.; Hammond, R. B.; Lai, X.; Roberts, K. J. Towards an Understanding of the Nucleation of Alpha-Para Amino Benzoic Acid from Ethanolic Solutions: A Multi-Scale Approach. *Faraday Discuss.* **2015**, *179*, 79−114.
(36) Turner, T. D.; Corzo, D. M. C.; Toroz, D.; Curtis, A.; Dos Santos, M. M.; Hammond, R. B.; Lai, X.; Roberts, K. J. The Influence of Solution Environment on the Nucleation Kinetics and Crystallisability of Para-Aminobenzoic Acid. *Phys. Chem. Chem. Phys.* **2016**, *18*, 27507−27520.
(37) Rosbottom, I.; Ma, C. Y.; Turner, T. D.; O'Connell, R. A.; Loughrey, J.; Sadiq, G.; Davey, R. J.; Roberts, K. J. Influence of Solvent Composition on the Crystal Morphology and Structure of P-Aminobenzoic Acid Crystallized from Mixed Ethanol and Nitromethane Solutions. *Crystal Growth Des.* **2017**, *17*, 4151−4161.
(38) Technobis. Crystal 16 https://www.crystallizationsystems.com/crystal16, (accessed February 5, 2019).
(39) Tang, X.; Kaskiewicz, P. L.; Camacho Corzo, D. M.; Lai, X.; Roberts, K. J.; Dowding, P.; More, I. Solubility and Crystallisability of the Ternary System: Hexadecane and Octadecane Representative in Fuel Solvents. *Fuel* **2018**, *226*, 665.
(40) Sangwal, M. *Additives and Crystallization Processes: From Fundamentals to Applications*; John Wiley & Sons Ltd.: Chichester, 2007.
(41) Camacho Corzo, D. M.; Borissova, A.; Hammond, R. B.; Kashchiev, D.; Roberts, K. J.; Lewtas, K.; More, I. Nucleation Mechanism and Kinetics from the Analysis of Polythermal Crystallisation Data: Methyl Stearate from Kerosene Solutions. *CrystEngComm* **2014**, *16*, 974−991.
(42) Jiang, S.; Ter Horst, J. H. Crystal Nucleation Rates from Probability Distributions of Induction Times. *Crystal Growth Des.* **2011**, *11*, 256−261.
(43) Black, J. *Solvent & Additive Effects on the Appearance of Polymorphs of P-Aminobenzoic Acid*; Ph.D. Thesis, The University of Manchester: Manchester, 2016.
(44) Nielsen, A. E.; Söhnel, O. Interfacial Tensions Electrolyte Crystal-Aqueous Solution, from Nucleation Data. *J. Cryst. Growth* **1971**, *11*, 233−242.
(45) Sullivan, R. A.; Davey, R. J.; Sadiq, G.; Dent, G.; Back, K. R.; Ter Horst, J. H.; Toroz, D.; Hammond, R. B. Revealing the Roles of Desolvation and Molecular Self-Assembly in Crystal Nucleation from Solution: Benzoic and p-Aminobenzoic Acids. *Crystal Growth Des.* **2014**, *14*, 2689−2696.
(46) Söhnel, O.; Mullin, J. W. A Method for the Determination of Precipitation Induction Periods. *J. Cryst. Growth* **1978**, *44*, 377−382.
(47) MacFhionnghaile, P.; Svoboda, V.; McGinty, J.; Nordon, A.; Sefcik, J. Crystallization Diagram for Antisolvent Crystallization of Lactose: Using Design of Experiments to Investigate Continuous Mixing-Induced Supersaturation. *Crystal Growth Des.* **2017**, *17*, 2611−2621.
(48) Feng, L.; Berglund, K. A. ATR-FTIR for Determining Optimal Cooling Curves for Batch Crystallization of Succinic Acid. *Crystal Growth Des.* **2002**, *2*, 449−452.
(49) Simone, E.; Saleemi, A. N.; Tonnon, N.; Nagy, Z. K. Active Polymorphic Feedback Control of Crystallization Processes Using a Combined Raman and ATR-UV/Vis Spectroscopy Approach. *Crystal Growth Des.* **2014**, *14*, 1839−1850.
(50) Li, R. F.; Penchev, R.; Ramachandran, V.; Roberts, K. J.; Wang, X. Z.; Tweedie, R. J.; Prior, A.; Gerritsen, J. W.; Hugen, F. M. Particle Shape Characterisation via Image Analysis: From Laboratory Studies to in-Process Measurements Using an in Situ Particle Viewer System. *Org. Process Res. Dev.* **2008**, *12*, 837−849.
(51) Gallagher, P. M.; Coffey, M. P.; Krukonis, V. J.; Klasutis, N. Gas Antisolvent Recrystallization: New Process To Recrystallize Compounds Insoluble in Supercritical Fluids. In *Supercritical Fluid Science and Technology*; Johnson, K. P., Penninger, J. M. L., Eds.; ACS Symposium Series: Washington DC, 1989; Vol. *406*, pp 334−354.
(52) Zauner, R.; Jones, A. G. Scale-up of Continuous and Semibatch Precipitation Processes. *Ind. Eng. Chem. Res.* **2000**, *39*, 2392−2403.
(53) Shekunov, B. Y.; Baldyga, J.; York, P. Particle Formation by Mixing with Supercritical Antisolvent at High Reynolds Numbers. *Chem. Eng. Sci.* **2001**, *56*, 2421−2433.

DOI: 10.1021/acs.oprd.9b00242
Org. Process Res. Dev. 2019, 23, 1948−1959